processes

MDPI

Article

Research on Adaptive Distribution Control Strategy of Braking Force for Pure Electric Vehicles

Jingang Liu [1, 2,*], Lei Bu [1], Bing Fu [1, 3,*], Gaosheng Wang [1, 2], Lihong He [2], Jianyun Zheng [1] and Yuliang Hu [1, 4]

[1] School of Mechanical Engineering and Mechanics, Xiangtan University, Xiangtan 411105, China;
[2] Key Laboratory of Automotive Power and Transmission System of Hunan Province, Xiangtan 411100, China
[3] Zhuzhou Gear Co., LTD,Zhuzhou 412000, China.
[4] Guangdong Shunde Weisi Robot Co., LTD,Foshan 528000, China.
* Correspondence: wellbuild@126.com, fubing@xtu.edu.cn

Abstract: The actual driving conditions of pure electric vehicles are complex and changeable. Limited by road adhesion conditions, it is necessary to give priority to ensuring safety and timely taking into account the energy recovery ratio of the vehicle during braking to obtain better braking quality. Therefore, a pure electric vehicle with EHB(Electro-Hydraulic Braking) system is taken as the research object, and its braking force adaptive distribution control strategy is studied. Firstly, based on the vehicle configuration and braking system scheme, the vehicle dynamics model including seven degrees of freedom, tire, drive motor, main reducer, battery pack, and braking system was constructed. Secondly, based on line I and ECE regulations, the adaptive braking force distribution control strategy was formulated by taking the maximum regenerative braking torque as the inflection point, the synchronous adhesion coefficient as the desired point, and the battery SOC, road adhesion coefficient, and braking strength as the threshold. Finally, the vehicle dynamics simulation model was built on the Matlab/ Simulink platform, and the simulation results verified the feasibility of the proposed braking force adaptive allocation control strategy. The research shows that the adaptive distribution control strategy can better adapt to the complex and variable driving conditions of the vehicle by combining the inflection point and the desired point. The braking energy recovery ratio of the vehicle under the NEDC and NYCC cycle conditions under the high adhesion road is 52.62% and 47.45%. The braking force distribution curve under the low adhesion extreme road is close to line I.

Keywords: electric vehicle; braking force; adaptive distribution control; regenerative braking; synchronous adhesion coefficient

Citation: Lastname, F.; Lastname, F.; Lastname, F. Title. *Processes* **2022**, *10*, x. https://doi.org/10.3390/xxxxx

Academic Editor: Firstname Lastname

Received: date
Accepted: date
Published: date

1. Introduction

The electric powertrain system is characterized by low emission and high efficiency, which is one of the effective ways to alleviate the energy crisis and environmental pollution in the long term [1-2]. Although there have been significant developments in motor control strategy and energy density management, there are still some problems such as low battery utilization efficiency, limited driving mileage and relatively long charging speed, which prevent the large-scale commercialization of battery-based electric vehicles [3-4].

Studies show that 25% of the total driving energy of electric vehicles is lost by friction braking into heat energy [5]. Regenerative braking is an effective method to convert braking energy into electric energy, which can effectively improve the driving range of trams, especially for pure electric and hybrid electric vehicles that mainly drive in urban conditions [6-7]. However, driving intention, braking intensity, vehicle speed, battery charging state and other factors will affect the use of regenerative braking effect. Therefore, the research on regenerative braking of electric vehicles is of great significance for promoting the large-scale commercialization of electric vehicles.

At present, the main research on regenerative braking is to rationally distribute braking force of front and rear wheels of automobiles, and dynamically coordinate energy recovery power and mechanical braking power. Under the premise of ensuring braking safety, regenerative braking performance of automobiles can be brought to the limit, so as to maximize braking energy recovery. In practical application, the braking force distribution method of the traditional automo-bile's front and rear wheels is mostly distributed by a fixed ratio approaching line I, the braking energy recovery is limited, and the automobile only realizes the ideal state of the front and rear wheels locked at the point of synchronous adhesion coefficient [8].

In recent years, a large number of commercial passenger vehicles have been loaded with proportional valves, high-speed on-off valves, and other braking force regulation devices, which can achieve variable ratio braking force distribution through the design of turning points, to achieve the best braking quality while leaving space for braking stability [9-10].Xu, G. et al. developed a strategy combining fuzzy rule based regenerative braking with tandem regenerative braking to make the braking force distribution curve between the front and rear wheels approximate the ideal distribution curve and improve the braking energy recovery efficiency [11]. Ma, Z. et al. proposed for the regenerative braking system of small four-wheel drive electric vehicles An improved braking energy recovery strategy based on I-line. This strategy covers a wider range of vehicle braking situations while prioritising braking stability [12]. Kumar, C.N. et al. proposed a new synergistic control of regenerative and friction braking together in hybrid electric vehicles, which makes the braking force distribution curves of the front and rear wheels closer to the ideal distribution curves and facilitates stable braking [13]. li S. et al. based on line ECE regulation and line I, the ratio of regenerative braking force to front axle braking force was designed according to different braking intensities, and a braking energy recovery control strategy was developed, which effectively improved the proportion of recovered braking energy [14]. Some studies have focused on braking force distribution strategies considering algorithms, hardware arrangement of braking schemes, attached ground and other situations. Ouyang et al. compared and analysed three braking force distribution control strategies, and the results showed that the braking force distribution scheme with tandem braking can effectively and maximally achieve braking energy recovery and reduce the energy consumption of the whole vehicle [15]. Ko, J. et al. integrated a regenerative braking cooperative control algorithm based on the whole vehicle braking force distribution strategy to improve the braking energy recovery ratio by increasing the gradient of the change of the target braking force relative to the pedal stroke [16]. Wei, Z. et al. developed a braking force coordination control strategy to effectively utilize the front axle regenerative braking force while the braking performance of the vehicle is guaranteed under low adhesion road surfaces [17]. Zhang, L. et al. proposed a regenerative braking control strategy for all braking conditions based on a new braking strength definition method, which can effectively The braking efficiency can be improved [18]. The above braking force distribution control strategies are formulated by dividing braking de-mand according to braking intensity under specific working conditions, and then combining braking regulations, motor and battery constraints. However, the actual working conditions of automobiles are complex and the road adhesion conditions are different. It is difficult to realize the maximum recovery of braking energy and take into account the braking safety at the same time when the braking force distribution is mainly based on the braking strength.

Therefore, on the basis of this article is in line I and ECE regulations, to maximize the regenerative braking torque as the turning point, and synchronous adhesion coefficient for expectations. Developed a comprehensive consideration of motor regenerative braking torque limit, the battery SOC and road adhesion coefficient and brake strength under braking force distribution of adaptive control strategy, to adapt to the car's complicated working condition, In this way, the energy recovery ratio of the vehicle can be taken into account while the braking safety is guaranteed.

The rest of this paper is organized as follows: The second chapter introduces the configuration of the electric vehicles and its braking system. The third chapter realizes the modelling of the vehicle dynamic model. In chapter 4, the adaptive control strategy of braking force distribution is introduced and the model is built. In Chapter 5, the adaptive distribution control strategy of braking force is simulated and analyzed. Finally, the conclusion is summarized in Chapter 6.

2.Vehicle configuration and braking system

The adopted vehicle configuration scheme is shown in Figure 1. The model is a pure electric vehicle, a front-drive vehicle, and the driving system adopts the current mainstream transmission scheme, that is, single motor drive and single stage reducer. The braking system abandons the traditional vacuum booster device, electric vacuum pump, and P-EHB scheme, and adopts the electric servo booster and the hydraulic regulating unit, which belongs to the two-box scheme.

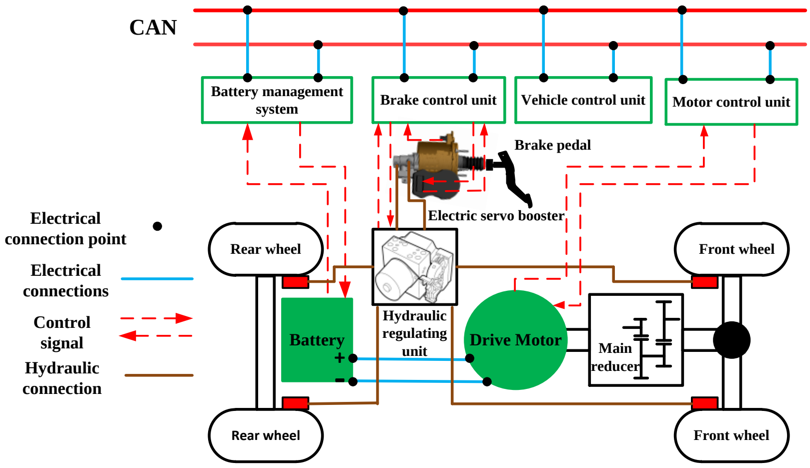

Figure 1. The vehicle configuration scheme

The structure of the adopted electric servo booster is shown in Figure 2. The booster is mainly composed of an input push rod, turbo worm, screw, return spring, tandem double chamber brake master cylinder and other parts.

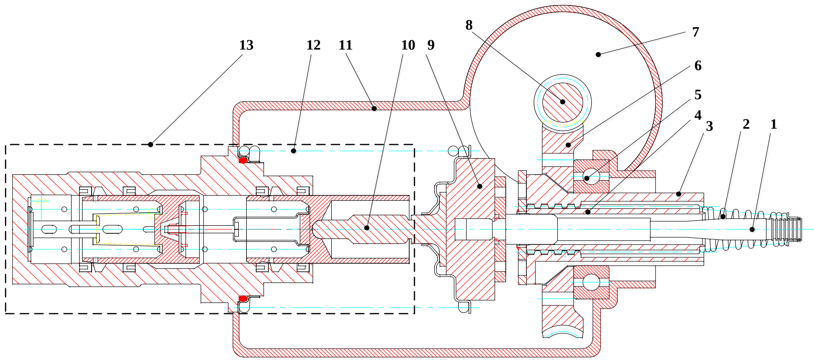

Figure 2. The electric servo booster structure

1—input push rod；2—cone spring；3—nut; 4—lead rod; 5—deep groove ball bearing; 6—turbowheel; 7—power motor mounting hole; 8—worm; 9—feedback disk; 10—master cylinder push rod; 11—Housing assembly; 12—return spring; 13—tandem double chamber brake master cylinder assembly.

Its working principle is as follows: when the booster is normal, the booster motor runs quickly to the specified position, the blocking torque is acted on the screw by the worm gear and worm, and the horizontal thrust is generated. The thrust and pedal forces are coupled to the master cylinder piston. Release the brake pedal, the power motor reverses to the specified position, and the return spring ensures that the brake pedal returns to the initial position. Booster failure, that is, the booster motor does not work, because there is a slide between the screw and the turbine, the pedal force directly through the cone spring, and the screw together to squeeze the feedback disk, so that the pedal force is transformed into the pressure of the master cylinder.

The hydraulic regulating unit is the current mainstream DSC/ESP scheme. The front braking and rear braking of the disc braking hydraulic regulating unit adopt an H-type double circuit, and its specific structure schematic diagram is shown in Figure 3.

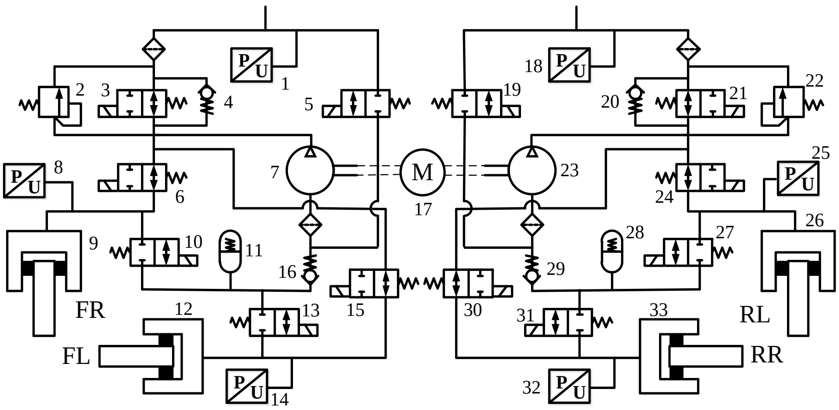

Figure 3. The schematic diagram of hydraulic regulatingunit

1, 8, 14, 18, 25, 32—pressure sensor; 4, 16, 20, 29—one-way valve; 2, 22—relief valve; 3, 21—isolation solenoid valve; 5, 19—adjusting unit inlet solenoid valve; 7, 17, 23—electric pump; 6, 15, 24, 30—wheel cylinder inlet solenoid valve; 10, 13, 27, 31—Wheel cylinder outflow solenoid valve; 11, 28—low pressure accumulator; 9, 12, 26, 33—wheel cylinder assembly.

3. Vehicle dynamics modeling

3.1 Vehicle 7-DOF model

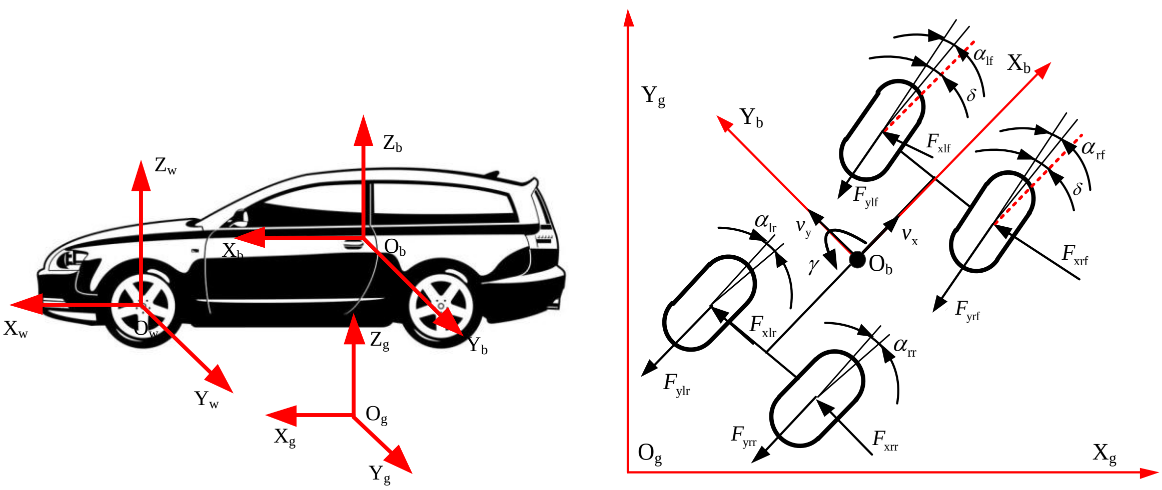

Figure 4. Schematic diagram of seven-degree-of-freedom vehicle model of four-wheel vehicle

As shown in Figure 4, the coordinate systems O_g-$X_gY_gZ_g$, O_w-$X_wY_wZ_w$, O_b-$X_bY_bZ_b$ are respectively established with the ground, wheel center and vehicle centroid to describe the actual motion state of the vehicle .When braking, the differential equations of the longitudinal, transverse and yaw motions along the longitudinal and transverse directions of the X_b axis and Y_b axis and the normal directions around the Z_b axis are as follows:

$$m(v_x' - v_y\gamma) = -(F_{xlf} + F_{xrf})\cos\delta - (F_{ylf} + F_{yrf})\sin\delta - F_{xlr} - F_{xrr} \tag{1}$$

$$m(v_y' + v_x\gamma) = -(F_{xlf} + F_{xrf})\sin\delta + (F_{ylf} + F_{yrf})\cos\delta + F_{ylr} + F_{yrr} \tag{2}$$

$$\begin{aligned} I_{zb}\gamma' = {} & -a(F_{xlf} + F_{xrf})\sin\delta - \frac{1}{2}d(F_{xrf} - F_{xlf})\cos\delta + a(F_{ylf} + F_{yrf})\cos\delta + \frac{1}{2}d(F_{ylf} - F_{yrf})\sin\delta \\ & -b(F_{ylr} + F_{yrr}) + \frac{1}{2}d(F_{xlr} - F_{xrr}) \end{aligned} \tag{3}$$

The side-deviation Angle $\alpha_i (i = \text{lf}, \text{rf}, \text{lr}, \text{rr})$ is:

$$\begin{cases} \alpha_{lf} = \arctan\dfrac{v_y + a\gamma}{v_x - 0.5d\gamma} - \delta \\ \alpha_{rf} = \arctan\dfrac{v_y + a\gamma}{v_x + 0.5d\gamma} - \delta \\ \alpha_{lr} = \arctan\dfrac{v_y - b\gamma}{v_x - 0.5d\gamma} \\ \alpha_{rr} = \dfrac{v_y + b\gamma}{v_x + 0.5d\gamma} \end{cases} \tag{4}$$

The vertical load of each wheel $F_{zi} (i = \text{lf}, \text{rf}, \text{lr}, \text{rr})$ is:

$$\begin{cases} F_{zlf} = m[\dfrac{gb}{2L} - v_x'\dfrac{h}{2L} - v_y'\dfrac{hb}{dL} - \dfrac{F_gh}{2mL}] \\ F_{zrf} = m[\dfrac{gb}{2L} - v_x'\dfrac{h}{2L} + v_y'\dfrac{hb}{dL} - \dfrac{F_gh}{2mL}] \\ F_{zlr} = m[\dfrac{ga}{2L} + v_x'\dfrac{h}{2L} - v_y'\dfrac{ha}{dL} + \dfrac{F_gh}{2mL}] \\ F_{zrr} = m[\dfrac{ga}{2L} + v_x'\dfrac{h}{2L} + v_y'\dfrac{ha}{dL} + \dfrac{F_gh}{2mL}] \end{cases} \tag{5}$$

The center speed of each wheel $v_i (i = \text{lf}, \text{rf}, \text{lr}, \text{rr})$ is:

$$\begin{cases} v_{lf} = (v_x - 0.5d\gamma)\cos\delta + (v_y + a\gamma)\sin\delta \\ v_{rf} = (v_x + 0.5d\gamma)\cos\delta + (v_y + a\gamma)\sin\delta \\ v_{lr} = v_x - 0.5d\gamma \\ v_{rr} = v_x + 0.5d\gamma \end{cases} \tag{6}$$

The rotation dynamics equation of each wheel is:

$$J_{wi}w_i' = F_{xi}R - T_{bi} \tag{7}$$

Each wheel slip rate $\lambda_i (i = \text{lf}, \text{rf}, \text{lr}, \text{rr})$ is:

$$\lambda_i = \frac{R\omega_i - v_i}{v_i} \times 100\% \tag{8}$$

where v_x is the longitudinal velocity of the vehicle; v_y is vehicle lateral speed; $F_{xi}(i = \mathrm{lf,rf,lr,rr})$ (lf stands for left front wheel; rf stands for right front wheel; lr stands for left rear wheel; rr stands for right rear wheel, and the subsequent meanings of the same Angle mark are uniform) is the longitudinal force of each wheel; $F_{yi}(i = \mathrm{lf,rf,lr,rr})$ is the lateral force of each wheel; $F_{zi}(i = \mathrm{lf,rf,lr,rr})$ is the vertical load of each wheel; γ is vehicle yaw Angle velocity; δ is the Angle of the left front wheel and the right front wheel; $\alpha_i(i = \mathrm{lf,rf,lr,rr})$ is the lateral deviation Angle of each wheel tire; m is vehicle mass; a,b,are the distances from the center of mass Ob of the vehicle along the longitudinal direction of X_b axis to the front and rear wheel rotating shafts respectively; $L=a+b$ is the wheelbase of the vehicle along the transverse direction of Y_b axis; I_{zb} is the moment of inertia of the vehicle about the Z_b axis; F_g is vehicle air resistance; h is the height of vehicle center of mass above the ground; R is wheel radius; $w_i(i = \mathrm{lf,rf,lr,rr})$ is the rotational angular velocity of each wheel; $J_{wi}(i = \mathrm{lf,rf,lr,rr})$ is the moment of inertia of each wheel; $T_{bi}(i = \mathrm{lf,rf,lr,rr})$ denotes the braking torque of each wheel.

3.2 Tire Model

The tire model is expressed by the MF tire formula, which can be expressed as [16] :

$$F(x) = D\sin\left\{C\arctan\begin{bmatrix}B(x+S_h)(1-E)\\+E\arctan(BX)\end{bmatrix}\right\}+S_v \tag{9}$$

When calculating the longitudinal force, the expression of the relevant variables is:

$$\begin{cases}D = b_1F_z^{\ 2}+b_2F_z\\C = b_0\\B = (b_3F_z^{\ 2}+b_4F)/[CD\exp(b_5F_z)]\\S_h = b_9F_z+b_{10}\\S_v = 0\\E = b_6F_z^{\ 2}+b_7F_z+b_8\end{cases} \tag{10}$$

When calculating the transverse force, the expression of the relevant variable is:

$$\begin{cases}D = a_1F_z^{\ 2}+a_2F_z\\C = a_0\\B = [a_3\sin(2\arctan(F_z/a_4))\times(1-a_5|\varphi|)]/(CD)\\S_h = a_8\varphi+a_9F_z+a_{10}\\S_v = a_{11}\varphi F_z+a_{12}F_z+a_{13}\\E = a_6F_z+a_7\end{cases} \tag{11}$$

where a_i、b_j(i=1~13、j=1~10) are the corresponding tire intrinsic coefficients.

3.3 Battery Model

The Rint internal resistance model is adopted for the battery model [20] . According to Kirchhoff's law, the voltage balance equation can be expressed as follows:

$$U_b = E_b - I_bR_b \tag{12}$$

Battery SOC value is the ratio of the remaining battery capacity to the total battery capacity, which can be expressed as follows:

$$SOC = (Ah_{max} - Ah_{used})/Ah_{max} \tag{13}$$

where E_b is the terminal voltage of the battery pack; I_b is the battery string line current; R_b is the internal resistance of battery pack; U_b is the open-circuit voltage of the battery string; Ah_{max} is the total battery capacity; Ah_{used} is the battery capacity consumption.

3.4 Powertrain model

Motor torque response usually has a hysteresis phenomenon. When the target motor torque is known, the actual output torque T_m of the motor can be expressed as follows:

$$\dot{T}_m = \frac{T_{mc} - T_m}{\tau} \tag{14}$$

The power demand of the driving motor can be expressed as follows:

$$P_m = T_m \bullet w_m \bullet \eta_m^{\operatorname{sgn}(T_m \bullet w_m)} \tag{15}$$

The maximum regenerative braking torque T_{reg} provided by the motor can be shown as follows [21]:

$$T_{reg} = \begin{cases} 9549P_e / n_e; n \le n_e \\ 9549P_e / n; n > n_e \end{cases} \tag{16}$$

The deceleration and torsional increase characteristics of the single speed ratio main reducer can be expressed as follows:

$$\begin{cases} w_{g\text{-}out} = \dfrac{w_m}{i} \\ T_{g\text{-}out} = \dfrac{T_m i}{\mu_1} \end{cases} \tag{17}$$

where τ is the motor torque lag time; w_m is the speed of the driving motor; η_m is the driving motor assembly efficiency; sgn is a sign function, with the value of ± 1, indicating that the driving motor is in the driving state or the braking state; n_e is the rated speed of the motor; P_e is the rated power of the motor; n is the actual speed of the motor; i is speed ratio of reducer; μ_1 is the reducer efficiency; $w_{g\text{-}out}$ is the output speed of the reducer; $T_{g\text{-}out}$ is the output torque of the reducer.

3.5 Braking system model

According to the ideal curve of pedal displacement and brake master cylinder oil pressure of an electric booster, the relationship between brake master cylinder oil pressure P_c and brake pedal displacement X can be fitted as follows [22]:

$$P_c = \begin{cases} 0.0237x^2 - 0.0335x - 0.0957 & x > 2.8 \\ 0 & x \le 2.8 \end{cases} \tag{18}$$

The increasing/decreasing/retaining pressure characteristics of P_w of brake wheel cylinder are as follows:

$$\frac{dP_w}{dt} = \frac{1}{C_{e1}R_{e1}}(P_c - P_w)^{k_1} \tag{19}$$

$$\frac{dP_w}{dt} = \frac{1}{C_{e2}R_{e2}}(P_w - P_r)^{k_2} \tag{20}$$

$$\frac{dP_{\mathrm{w}}}{dt}=0 \tag{21}$$

where P_{r} is the accumulator pressure, which can be neglected.The values of C_{e1}、R_{e1}、C_{e2}、R_{e2}、k_1、k_2 and other parameters [23] are shown in Table 1 below:

Table 1. The parameter selection of braking system

parameter	The numerical	parameter	The numerical
$1/(C_{e1}R_{e1})$	37.5342	$1/(C_{e2}R_{e2})$	38.3128
k_1	0.589	k_2	0.936

The braking torque of the brake wheel cylinder is:

$$T_{\mathrm{b}}=\frac{\mu_{\mathrm{b}}r_{\mathrm{b}}}{4}\pi(d_{\mathrm{w}})^2(P_{\mathrm{w}}-P_0)(t-\tau) \tag{22}$$

where μ_{b} is efficiency factor; r_{b} is the effective radius of braking wheel action; d_{w} is the effective radius of piston of brake wheel cylinder; P_0 is prepressure of brake wheel cylinder; τ is the braking torque output lag time.

4. Adaptive distribution control strategy of braking force

In order to give consideration to higher energy recovery ratio, superior braking safety, and better utilization of road adhesion, When formulating the braking force distribution strategy of the whole vehicle, it is necessary to combine the line f group with the front wheel locked and the rear wheel not locked, the line r group with the front wheel not locked and the rear wheel not locked, the line I with the front wheel locked and the rear wheel locked at the same time, the line ECE with the front wheel locked and the rear wheel not locked, and the line ECE with the front wheel not locked and the rear wheel locked. The corresponding expressions are as follows:

$$\begin{cases} F_{\mu1}=\varphi\dfrac{G}{L}(b+zh) \\ F_{\mu2}=Gz-F_{\mu1} \end{cases} \tag{23}$$

$$\begin{cases} F_{\mu1}=Gz-F_{\mu2} \\ F_{\mu2}=\varphi\dfrac{G}{L}(a-zh) \end{cases} \tag{24}$$

$$F_{\mu2}=\frac{1}{2}\left[\frac{G}{h}\sqrt{b^2+\frac{4hL}{G}F_{\mu1}}-(\frac{Gb}{h}+2F_{\mu1})\right] \tag{25}$$

$$\begin{cases} F_{\mu1}=\dfrac{z+0.07}{0.85}\dfrac{G}{L}(b+zh) \\ F_{\mu2}=Gz-F_{\mu1} \end{cases} \tag{26}$$

$$\begin{cases} F_{\mu1}=Gz-F_{\mu2} \\ F_{\mu2}=\dfrac{z+0.07}{0.85}\dfrac{G}{L}(a-zh) \end{cases} \tag{27}$$

where $F_{\mu1}$ is the front wheel braking force; $F_{\mu2}$ is the braking force of the rear wheel; G is the weight of the vehicle; z is braking strength; φ is the road adhesion coefficient.

The braking force distribution of the vehicle under a fixed load of 1.6T of the vehicle's curb mass is shown in Figure 5 below.

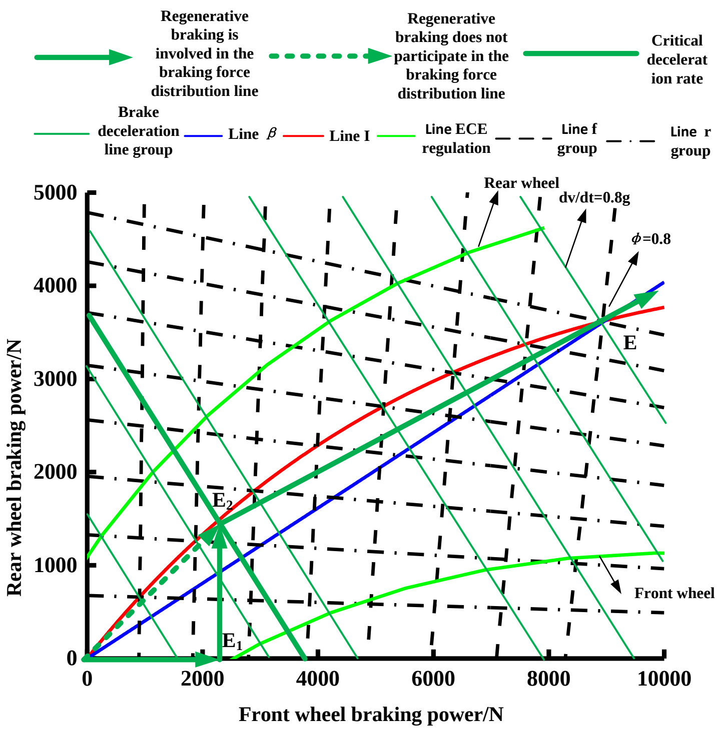

Figure 5. The braking force distribution basis diagram

Under different road adhesion coefficients and braking strengths, the line β will deviate from the line I greatly, and it is difficult to take into account the higher energy recovery ratio, superior braking safety, and better road adhesion utilization. Considering the control cost, difficulty, and other factors, and based on the characteristics of variable ratio braking force distribution, the key difficulty lies in how to choose the turning point with a higher degree of adaptation to achieve the vehicle braking force distribution curve approximating line I under a certain fixed load. Therefore, this paper proposes to design a front and rear wheel braking force distribution curve by using the intersection point of line β and line I (expected point E), namely the synchronous adhesion coefficient point, combining with the maximum regenerative braking force point of the driving motor and the mapping point of E1 point on line I, point E2, as shown in Figure 5.

The braking force distribution mode is selected according to the maximum road adhesion coefficient , which is OE1E2E orientation or OE2E orientation. On medium or high adhesion roads, when the braking force distribution curve is close to line I, a high energy recovery ratio should be taken into account. The braking force distribution ratio is OE1E2E orientation: when braking deceleration is located in OE1, the corre-sponding braking force is provided by the front wheel. When the braking deceleration is located in E1E2, the rear wheel braking force is distributed according to the second fixed distribution coefficient β_2.When the braking decel-eration is located within E2E, the front and rear wheel braking forces are distributed according to the first fixed dis-tribution coefficient β_1. For low adhesion road surfaces or extreme road surfaces, the braking force distribution curve should be infinitely close to the line I, and the braking force distribution ratio should be OE2 orientation: when the braking deceleration is located in OE2, the front and rear braking forces are distributed according to the third fixed distribution coefficient β_3.

Among them, the first fixed distribution coefficient β_1, the second fixed distribution coefficient β_2 and the third fixed distribution coefficient β_3 are determined by the following formula:

$$\beta_1 = \frac{y_{\mathrm{E}} - y_{\mathrm{E2}}}{x_{\mathrm{E}} + y_{\mathrm{E}} - x_{\mathrm{E2}} - y_{\mathrm{E2}}} \tag{28}$$

$$\beta_2 = \frac{y_{\mathrm{E2}} - y_{\mathrm{E1}}}{x_{\mathrm{E2}} + y_{\mathrm{E2}} - x_{\mathrm{E1}} - y_{\mathrm{E1}}} \tag{29}$$

$$\beta_3 = \frac{y_{\mathrm{E2}}}{x_{\mathrm{E2}} + y_{\mathrm{E2}}} \tag{30}$$

where $x_{\mathrm{E}}, y_{\mathrm{E}}$ *are the coordinates of point* E; $x_{\mathrm{E1}}, y_{\mathrm{E1}}$ *is the coordinate of* E1 *point;* $x_{\mathrm{E2}}, y_{\mathrm{E2}}$ *are the coordinates of* E2.

The braking deceleration corresponding to the E1 point was defined as the critical point of mild braking (0.152g). Point E2 was used as a parallel line paralleling to the braking deceleration line group, and this parallel line was de-fined as the moderate braking critical point (0.245g). Make a parallel line parallel to the braking deceleration line group through E2 point, and define the parallel line as the critical point of medium braking (0.245g).Therefore, the deceleration area of the vehicle where the light braking is located can be 0<du/dt≤0.152g, the moderate braking can be 0.152g<du/dt≤0.245g, and the high-intensity braking can be du/dt>0.245g. Combined with the SOC value of the vehicle, the corresponding front, and rear wheel braking force distribution principle is shown in Figure 6.

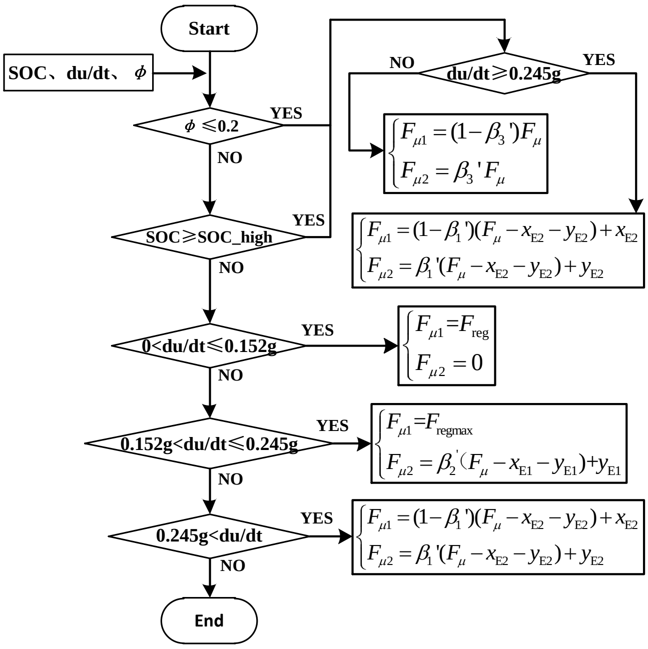

Figure 6. The adaptive distribution principle of braking force in front and rear wheels

The front wheel braking force is the sum of motor regenerative braking force and front wheel hydraulic braking force.When the vehicle speed is low, the speed correction factor is generally used to describe the process in which the front wheel hydraulic braking force gradually replaces the motor regenerative braking force. The speed correction factor k_1 can be expressed as:

$$k_1 = \begin{cases} 0; w_{\mathrm{m}} \le 38.5 rad/s \\ \dfrac{w_{\mathrm{m}} - 38.5}{76.5}; 38.5 rad/s < w_{\mathrm{m}} \le 115 rad/s \\ 1; w_{\mathrm{m}} > 115 rad/s \end{cases} \tag{31}$$

When the SOC value of the automobile battery is high, the SOC correction factor can be used to describe whether the SOC value of the vehicle reaches the upper limit, which can be used as a sign to enable the regenerative braking function of the motor.The speed correction factor k_2 can be expressed as:

$$k_2 = \begin{cases} 1; SOC \le 0.88 \\ 50(0.9 - SOC); 0.88 < SOC \le 0.9 \\ 0; SOC > 0.9 \end{cases} \tag{32}$$

Therefore, under the regenerative braking torque T_{reg} of the motor, the regenerative braking force provided to the wheel can be modified as follows:

$$F_{\mathrm{reg}} = \frac{T_{\mathrm{reg}} \cdot i \cdot \eta_1 \cdot k_1 \cdot k_2}{R} \tag{33}$$

Therefore, based on the above adaptive braking force distribution principle of front and rear wheels, combined with the vehicle speed and anti-lock requirements of each wheel, the adaptive braking force distribution control strategy is formulated.

As shown in Figure 7 where, u is vehicle speed; u_{min} and u_{stp} are critical regeneration speed (15km/h) and critical stopping speed (5km/h). To determine whether the wheel is locked is based on the optimal slip rate under the corresponding working conditions.

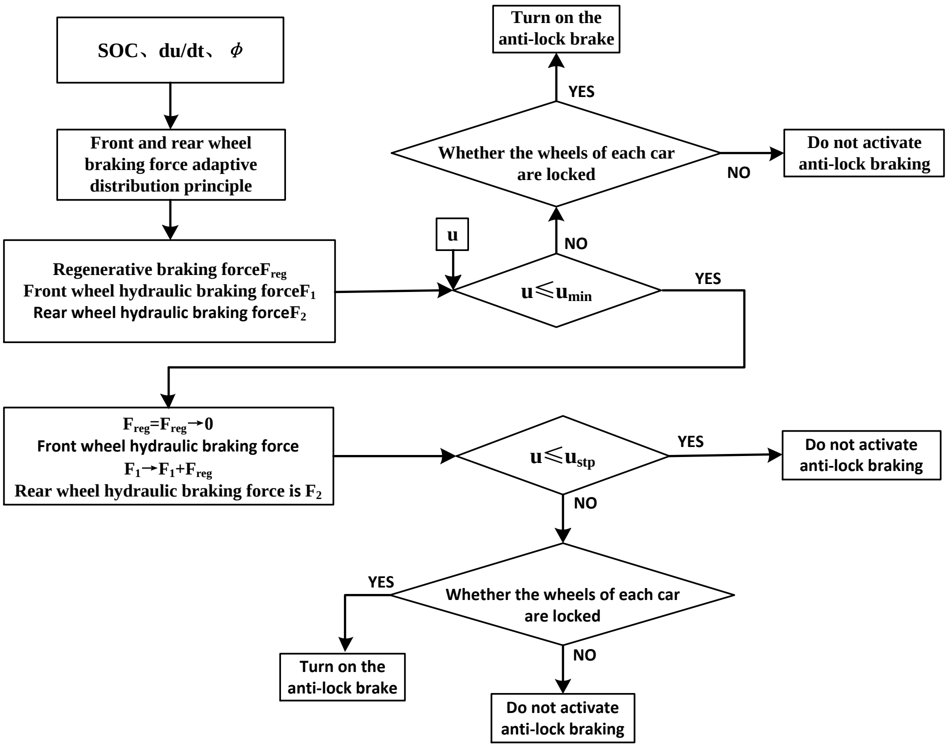

Figure 7. The control strategy of vehicle braking force adaptive distribution

5 Simulation Analysis

5.1 Vehicle Parameters

Based on the above vehicle dynamics model, in order to verify the proposed braking force adaptive allocation control strategy, this paper established its simulation model on the MATLAB/Simulink platform, and the basic parameters of the vehicle simulation adopted are shown in Table 2.

Table 2. The basic parameters of vehicle

The basic parameters	**The numerical**	**The basic parameters**	**The numerical**
Curb weight	1600kg	Maximum motor power	135 Kw
Windward area	2.58m2	Maximum motor speed	12000rpm
Total battery capacity	259Ah	Maximum motor torque	300 N.m
Speed ratio of reducer	8.55	The wheel radius	0.307m
Front/rear wheel radius	0.307m	Effective radius of rear wheel action	0.11 m
Effective radius of front wheel action	0.122m	Height of vehicle center of mass above	0.52 m
Distance from center of mass to front axle	1.208m	Distance from center of mass to rear axle	1.542 m

5.2 Simulation results of NEDC and NYCC cycle conditions with high attachment

The NEDC and NYCC cycle conditions of high adhesion road surface (with regenerative braking function involved in light braking and moderate braking) were respectively simulated and analyzed, and the results are shown in Figures 8-9 below. In the NEDC cycle condition, the initial SOC of the battery is 0.9. The braking behavior of the vehicle is light braking, and the corresponding brake pedal displacement is shown in Figure 8a). The maximum brake pedal displacement is 21.4mm. The braking deceleration is less than or equal to 0.152g. The regenerative braking torque of the driving motor is sufficient for service braking, and the maximum regenerative braking torque is 82N.m, which is less than the maximum regenerative braking torque of the driving motor. The deceleration of the whole vehicle can track the target value well and meet the target braking demand of the vehicle driver. A typical braking process period of the 1150s to 1160s is selected, as shown in Figure 8f). The regenerative braking torque of the driving motor can meet the braking requirements in the early stage of braking. However, since the vehicle needs to slow down to stop, the vehicle braking recovery function at the speed of 15km/h requires the whole vehicle friction torque to gradually replace the regenerative braking torque, and the front wheel generates braking pressure to gradually replace regenerative braking torque.

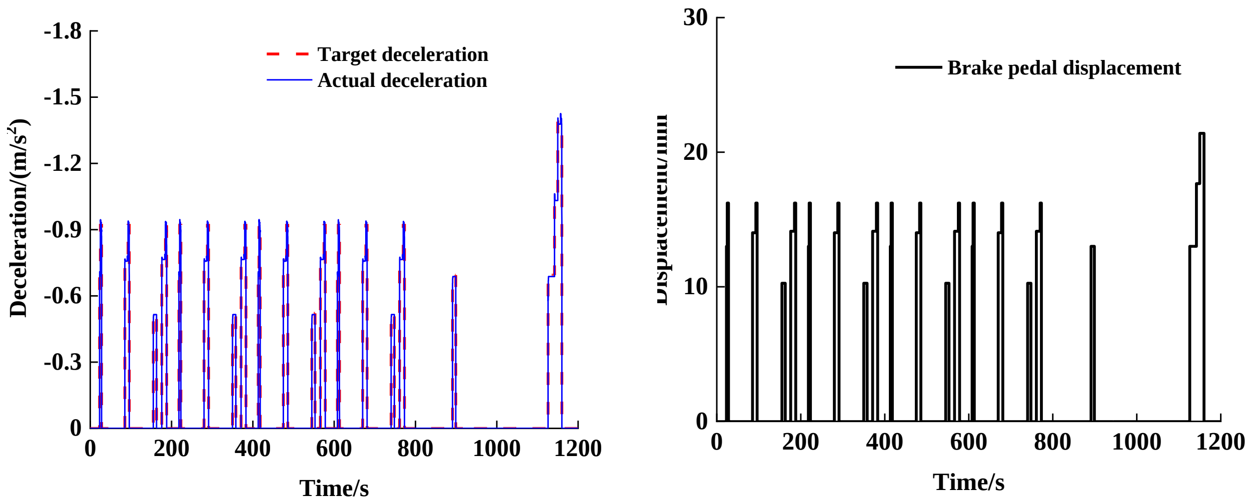

a）Brake deceleration b）Brake pedal displacement

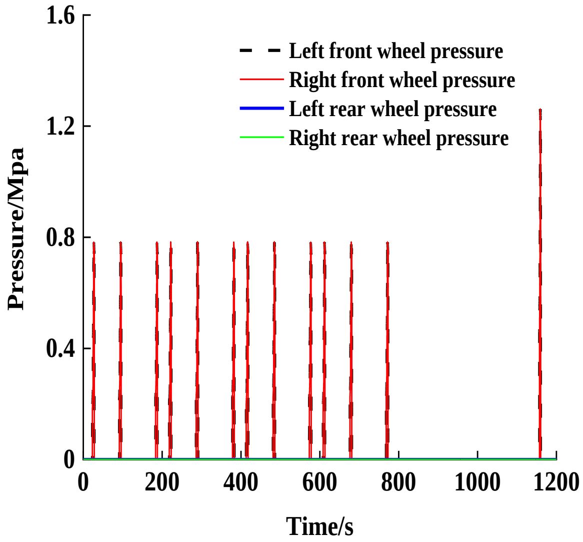

c）Brake pressure

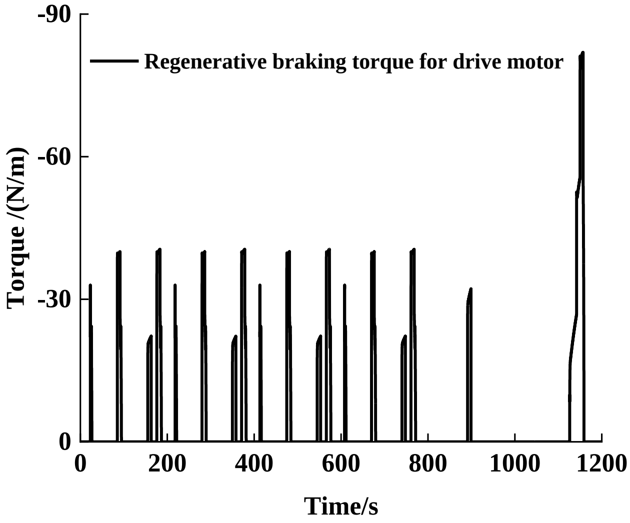

d）Regenerative braking torque for drive motor

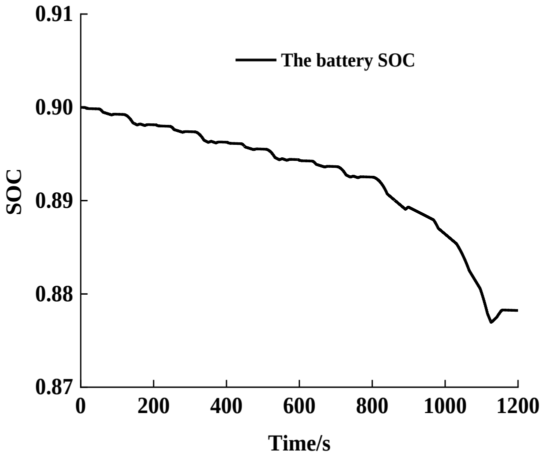

e）The battery SOC

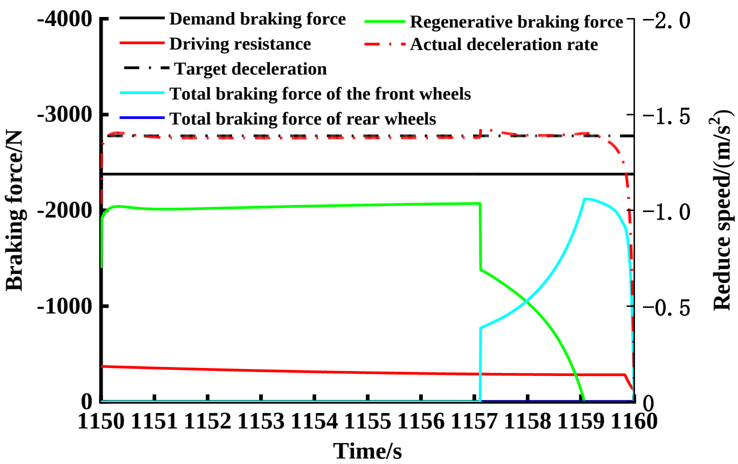

f）Braking force distribution in 1150~1160s

Figure 8. The simulation results of high adhesion NEDC cycle conditions

In NYCC cycle conditions, the braking behavior of the vehicle involves light braking, medium braking, and high-intensity braking. The corresponding brake pedal displacement is shown in Figure 9a), and the maximum brake pedal displacement is 30mm. The maximum braking deceleration is 2.64m/ S2, and about 3.96% of braking conditions have braking deceleration greater than 0.152g, which is the threshold of mild braking. In these conditions, the regenerative braking torque of the driving motor is not enough to maintain the service braking. The period of continuous braking to stopping within 552~563s is selected for analysis, as shown in Figure 9f). The system before 557s is mild, and the regenerative braking torque of the driving motor can provide all braking torque. After that it is medium braking, the vehicle speed will be lower than 15km/h at 558.5s, and the front wheel friction braking torque will gradually replace the regenerative braking torque of the driving motor until the vehicle speed is reduced to 5km/h,when the regenerative braking function is completely withdrawn.

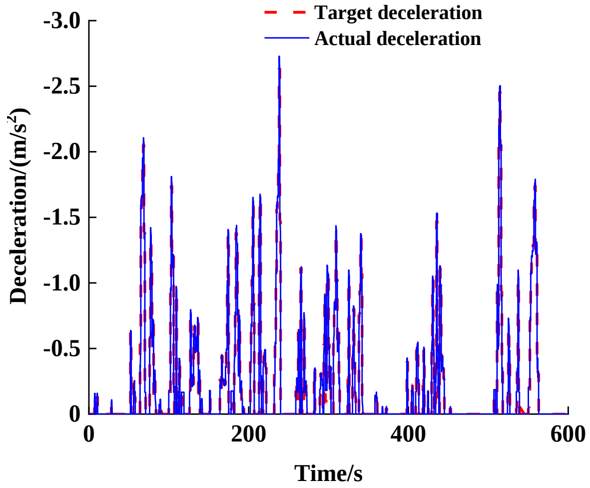

a） Brake deceleration

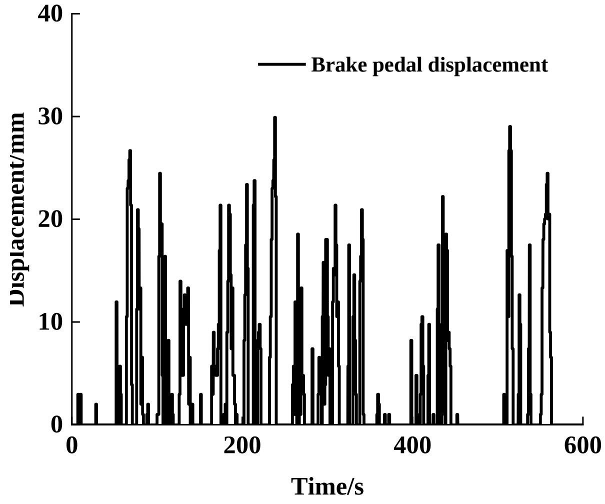

b） Brake pedal displacement

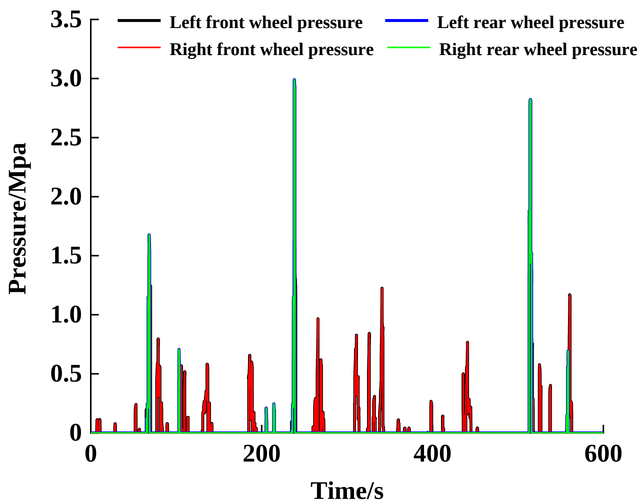

c） Brake pressure

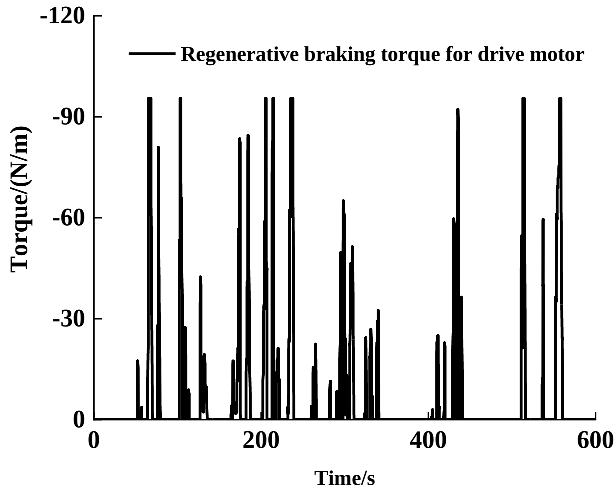

d） Regenerative braking torque for drive motor

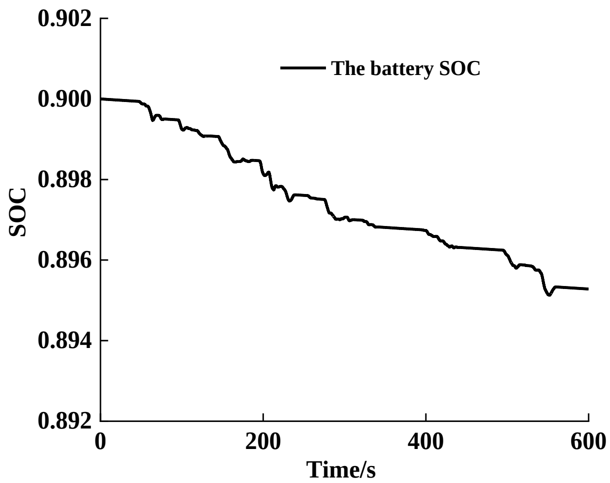

e） The battery SOC

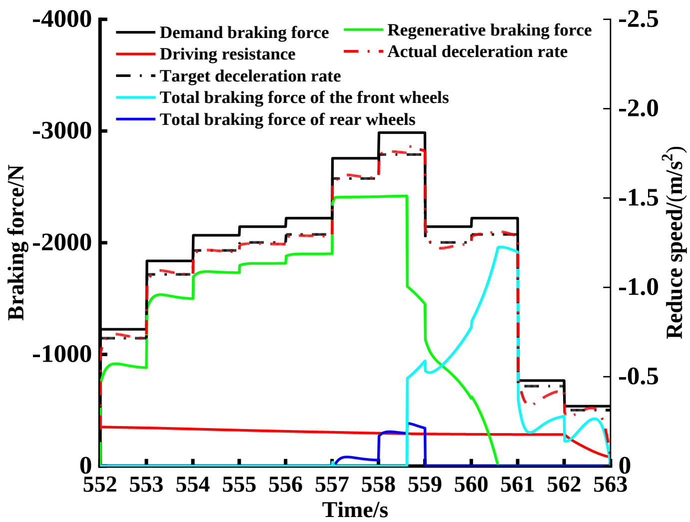

f） Braking force distribution in 552~ 563S

Figure 9. The simulation results of high adhesion NYCC cycle conditions

In order to further quantify the specific situation of regenerative braking energy recovery of the vehicle regenerative braking and anti-lock braking integrated control strategy proposed in this paper, the kinetic energy of the vehicle braking is calculated and compared with the electric energy stored by the battery. The calculation formula is as follows:

$$E_1 = \frac{1}{2} m (v_1^2 - v_0^2) \tag{34}$$

$$E_2 = \int_0^t U_{bf} \cdot I_{\mathrm{bf}} dt \tag{35}$$

Where E_1 is the total braking energy under a certain braking demand; E_2 is the braking energy actually recovered by the battery under a certain braking demand; v_1 is the final velocity under a certain braking demand; v_0 is the initial speed under a certain braking demand; U_{bf} is the open circuit voltage when a certain braking demand is delegated. I_{bf} is the discharge current under a certain braking demand.

The results of vehicle braking energy recovery are shown in Table 3 below.

Table 3. The results of finite element analysis

Comparing the results	Driving cycles	
	NEDC	NYCC
Total braking energy/kj	1962.72	936.99
Recoverable energy/kj	1032.75	444.56
Recovery of energy/%	52.62	47.45

5.3 Simulation results of extremely low adhesion road surface

The extreme ice pavement with an adhesion coefficient of 0.1 is simulated.According to analysis, the control interval of slip rate is 0.01-0.05, and the optimal slip rate is 0.03 [24]. Among them, the vehicle speed is 30km/h, and the braking deceleration speed is 0.12g. The results are shown in Figure 10.

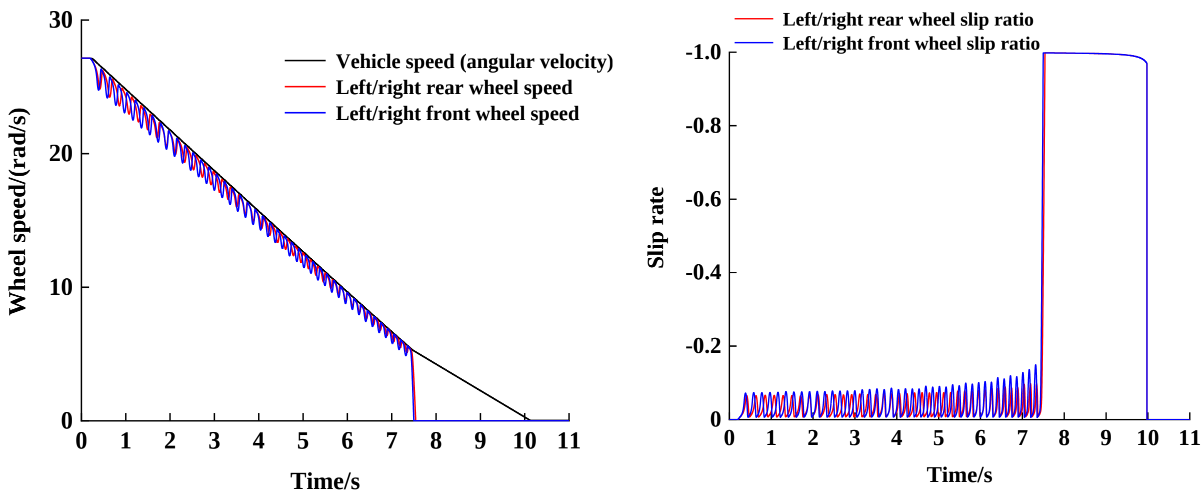

a）speed　　　b）Slip rate

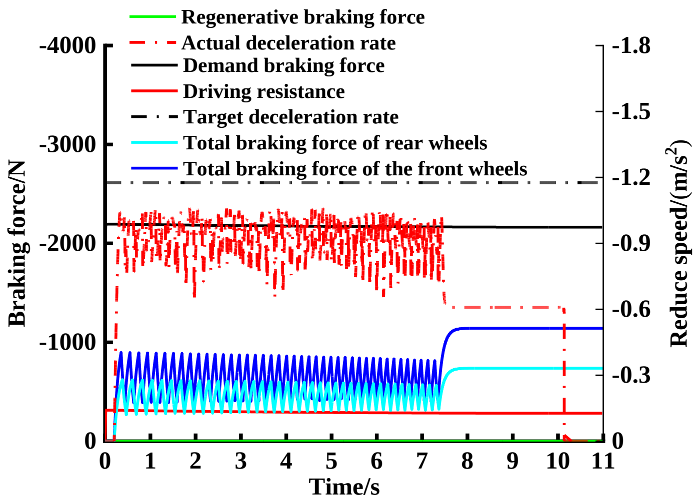

c）Braking force distribution

Figure 10. The simulation results of low adhesion road surface

Under the condition of road adhesion, the front and rear wheels of the vehicle have the risk of locking. To ensure the braking safety, the regenerative braking function is closed. This strategy can adjust the pressure according to the optimal slip rate control interval of 0.15~0.19 to ensure that the four wheels of the vehicle speed above 5km/h will not be locked, so that the vehicle can maximize the use of road adhesion for braking, greatly improve the braking safety of the vehicle, and prevent the wheel and tire from sliding when driving.

5.4 Braking force distribution results

Through the analysis of other braking deceleration conditions, combined with the above NEDC, NYCC, and extreme low adhesion road conditions of front and rear wheel braking force distribution, the corresponding vehicle braking force distribution is shown in Figure 11 below.

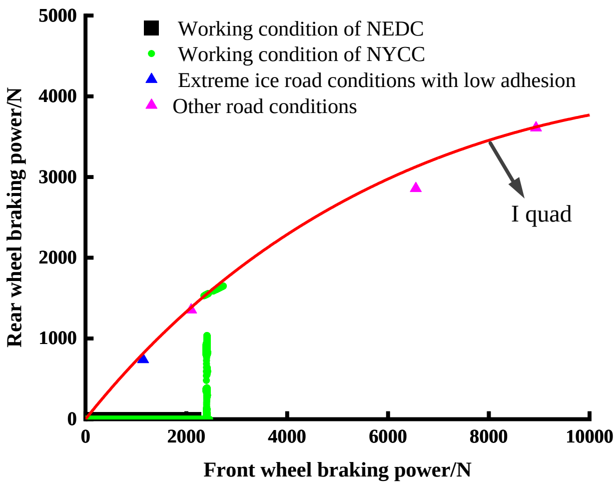

Figure 11. The distribution situation of braking force distribution

It can be seen from Figure 11 that the braking force distribution of the vehicle can be reasonably distributed according to the expected distribution mode. The braking force distribution point of the vehicle is closer to line I under the extremely low adhesion road surface, and the braking safety is also taken into account while the braking energy is recovered to the maximum extent under other working conditions.

6. Conclusion

1) Based on the configuration scheme of a pure electric vehicle, the vehicle dynamics model is established. On the ba-sis of Line I and ECE regulations, combined with the driver's total braking demand, road adhesion coefficient, battery SOC and other constraints, the adaptive distribution control strategy of braking force is formulated using the maximum regenerative braking torque and synchronous adhesion coefficient.

2) The simulation analysis of NEDC and NYCC cycle conditions under high adhesion road surface shows that the braking energy recovery ratio of the vehicle reaches 52.62% and 47.45%, respectively. Under the premise of brake safety, the braking energy recovery of the vehicle is maximized.

3) The simulation results under extreme low adhesion road and high braking strength show that the braking force distribution points of front and rear wheels of the vehicle can be effectively switched according to the adhesion coefficient of the road, which is basically consistent with line I, ensuring the safety priority principle of the vehicle braking, and greatly improving the braking quality of the vehicle under extreme bad working conditions.

Author Contributions: Data curation, J.L.; methodology, L.H. , J.L.; resources, J.L.; supervision, B.F.; visualization, G.W. , L.B.; writing—original draft, L.B.; writing—review & editing, Y.H. All authors have read and agreed to the published version of the manuscript.

Funding: The research was funded by National Natural Science Foundation of China: 52075465 ,The science and technology innovation Program of Hunan Province: 2020RC4038, National Natural Science Foundation of China:52105069, China Postdoctoral Science Foundation: 2021M703787, Outstanding Youth Fund of Hunan Provincial Department of Education: 21B0106.

Institutional Review Board Statement: No applicable.

Informed Consent Statement: Not applicable.

Data Availability Statement: The data are available from the authors upon reasonable request.

Conflicts of Interest: The authors declare no conflict of interest.

References

1. Kwon,K.; Minsik,S.; Seungjae,M. Efficient multi-objective optimization of gear ratios and motor torque distribution for electric vehicles with two-motor and two-speed powertrain system. *Applied Energy* **2020**, 259,114190.
2. Wang,F.; Zhang,J.; Xu,X.; Cai,Y.; Zhou,Z.; Sun,X. A comprehensive dynamic efficiency-enhanced energy management strategy for plug-in hybrid electric vehicles, *Applied Energy* **2019**, 247, 657–669.
3. Xu,X.; Zhao,J.; Zhao,J.; Shi,K.; Dong,P.; Wang,S.; Liu,Y.; Guo,W.; Liu,X. Comparative study on fuel saving potential of series-parallel hybrid transmission and series hybrid transmission, *Energy Conversion and Management* **2022**, 252, 114970.
4. Xiao,B.; Lu,H.; Wang,H.; Ruan,J.; Zhang,N. Enhanced Regenerative Braking Strategies for Electric Vehicles: Dynamic Performance and Potential Analysis. *Energies* **2017**, 10, 1875.
5. Ruan,J.; Walker,P.; Watterson,P.; Zhang,N. The dynamic performance and economic benefit of a blended braking system in a multi-speed battery electric vehicle.*Applied energy* **2016**,183,1240-1258.
6. Geraee,S.; Mohammadbagherpoor,M.; Shafiei,M.; Valizadeh,M.; Montazeri,F.; Feyzi,M.R. Regenerative braking of electric vehicle using a modified direct torque control and adaptive control theory.*Computers & Electrical Engineering* **2018**, 69 ,85–97.
7. Qin,Y.; Tang,X.; Jia,T.; Duan,Z.; Zhang,J.; Li,Y.; Zheng,L. *Noise and vibration suppression in hybrid electric vehicles: state of the art and challenges.Renewable and Sustainable Energy Reviews* **2020**,124 ,109782.
8. Yu,Z.*Automobile Theory*.; Mechanical Industry Press : Beijing, China, **2018**; pp. 134-142.
9. Lian,Y.; Zhao,Y.; Hu,L.; Tian,Y. Longitudinal collision avoidance control of electric vehicles based on a new safety distance model and constrained-regenerative-braking-strength-continuity braking force distribution strategy. *IEEE Transactions on Vehicular Technology* **2015**, 65, 4079-4094.
10. Wang,C.; Zhao,W.; Li,W. Braking sense consistency strategy of electro-hydraulic composite braking system. *Mechanical Systems and Signal Processing* **2018**, 109, 196-219.
11. Xu,G.; Li,W.;Xu,K.; Song,Z. An Intelligent Regenerative Braking Strategy for Electric Vehicles. *Energies* **2011**, 4, 1461-1477.
12. Ma,Z.; Sun,D. Energy recovery strategy based on ideal braking force distribution for regenerative braking system of a four-wheel drive electric vehicle. *IEEE access* **2020,** 8, 136234-136242.

13. Kumar,C. N.; Subramanian,S. C. Cooperative control of regenerative braking and friction braking for a hybrid electric vehicle. Proceedings of the Institution of Mechanical Engineers. *Journal of Automobile Engineering* **2016**, 230, 103-116.
14. Li,S.; Yu,B.; Feng,X. Research on braking energy recovery strategy of electric vehicle based on ECE regulation and I curve. *Science Progress* **2020**, 103, 0036850419877762.
15. Lu,D.;Ouyang,M.;Gu,j. Optimal Regenerative Braking Control for Permanent Magnet Synchronous Motors in Electric Vehicles.*Proceedings of the CSEE* **2013,** 33, 83-91.
16. Ko,J.; Ko,S.; Son,H.; Yoo,B.; Cheon,J.; Kim,H. Development of brake system and regenerative braking cooperative control algorithm for automatic-transmission-based hybrid electric vehicles. *IEEE Transactions on Vehicular Technology* **2014**, 64, 431-440.
17. Wei,Z.; Xu,J.; Halim,D. Braking force control strategy for electric vehicles with load variation and wheel slip considerations. *IET Electr. Syst. Transp* **2017**, 7, 41-47.
18. Zhang,L.; Cai,X. Control strategy of regenerative braking system in electric vehicles. *Energy Procedia* **2018**, 152, 496-501.
19. Li,L;Jia,G;Song,J;et al. Progress on Vehicle Dynamics Stability Control System. *Journal of Mechanical Engineering* **2013**, 49, 95-107.
20. Johnson,V.H. Battery performance models in ADVISOR. *Journal of Power Sources* **2022**, 110, 321-329.
21. Li,G.;Lin,Y;He,H. Regenerative Braking Control Strategy for Electric Vehicle.*Transactions of Beijing Institute of Technology* **2009**, 29, 520-524.
22. Yong,J.;Gao,F.;Ding,N. Design and Validation of an Electro-Hydraulic Brake System Using Hardware-in-the-loop Real-time Simulation.International *Journal of Automotive Technology* **2017**, 18, 603-612.
23. Zhao,Z.;Peng,Y. Simulation on Series Electro-hydraulic Combined Braking for 4WD Hybrid Electric *Car.Journal of System Simulation* **2012**, 24, 208-215.
24. Ma,Y.;Zhao,J.; Zhao,H.; Lu,C.; Chen,H. MPC-based slip ratio control for electric vehicle considering road roughness. *IEEE Access* **2019,** 7, 52405-52413.